THE JOURNAL OF PHYSICAL CHEMISTRY C

Article

Cite This: J. Phys. Chem. C 2017, 121, 23716-23726

pubs.acs.org/JPCC

Dynamic Three-Dimensional Nanowetting Behavior of Imidazolium-Based Ionic Liquids Probed by Molecular Dynamics Simulation

Yongji Guan,[†] Qunfeng Shao,[†] Wenqiong Chen,[†] Shimin Liu,[‡] Xiaoping Zhang,*[,†] and Youquan Deng*[,‡]

[†]Institute of Modern Communication, School of Information Science and Engineering, Lanzhou University, Lanzhou, 730000, People's Republic of China

[‡]Centre for Green Chemistry and Catalysis, Lanzhou Institute of Chemical Physics, Chinese Academy of Sciences, Lanzhou, 730000, People's Republic of China

Supporting Information

ABSTRACT: The dynamic three-dimensional nanowetting behavior of nanodroplets of three kinds of 1-ethyl-3-methylimidazolium ionic liquids (ILs) with radii between 10 and 30 Å is probed by molecular dynamics (MD) simulation on a solid silicon surface at temperatures ranging from 300 to 500 K. The simulation results show that contact angles change greatly and then tend to be saturated from 45° to 75° as the droplet radius of ILs varied from 10 to 20 Å and further to >20 Å. The values of the contact angle are anisotropic and could be 39.5° and 48.7° in the x and y directions of the droplets spreading on the solid silicon surface when the radius of the IL droplet is 10 Å, and increasing the radius of the droplets can weaken the anisotropy of the contact angle. Further analysis of the interaction among cations, anions, and silicon suggests that the van der Waals (VDW) interaction of ions and silicon substrate varies from −56.5 to −53.5 kJ/mol per ion pair and silicon, and the Coulombic interaction of cations and anions varies from −265.3 to −282.0 kJ/mol per ion pair as the droplet radius of ILs ranged from 10 to 30 Å. Upon increasing the droplet radius, the imidazolium ring of the cation in the adsorbed layer is more nearly parallel to the silicon substrate, and this allows a very effective interaction with the silicon substrate. These changes in the structure of the adsorbed layer in the vicinity of the silicon surface and their effects on the structuring of ions in the bulk liquid layers above this strongly adsorbed layer lead to the difference of VDW and Coulombic interactions as the droplet radius of ILs varied from 10 to 30 Å. Additionally, the impact of the intrinsic viscosity and temperature on the nanowetting behavior of ILs is also investigated.

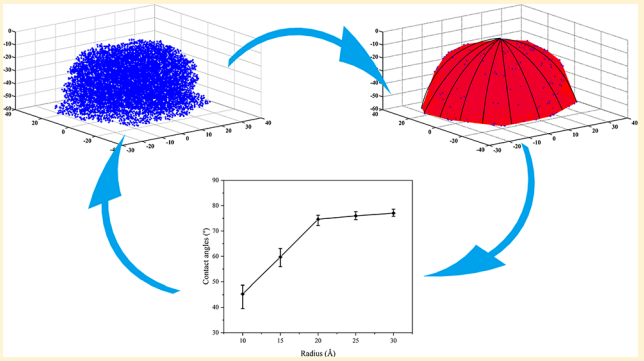

INTRODUCTION

Ionic liquids (ILs) are an emerging class of organic salts that are made entirely of specific cations and anions, but they have melting points close to room temperature and are known as room temperature ionic liquids (RTILs).[1−4] The physicochemical properties of ILs can be easily manipulated by tuning the functionalization and/or the combination of the cations and anions for task-specific applications.[3,5−8] ILs have been widely applied in variable-focus lenses,[9,10] lab on a chip,[11] and flow-induced energy harvesting[12,13] because of their excellent physicochemical properties. Meanwhile, due to the advent of nanoscience and nanotechnology, there has been a large amount of research to investigate the properties of bulk, pure ILs combining extended X-ray absorption fine structure (EXAFS) spectroscopy and molecular dynamics (MD) simulation on the nanoscale, and abundant results have been produced.[14−17] These promote emergence of a new class of composites consisting of nanoconfined ILs, which have the intrinsic chemistries of ILs and the original functions of solid matrices and then further endow ILs more extensive application to catalytic systems, CO_2 capture and separation, and ionogels as solid electrolytes and optical materials.[18]

Wetting phenomenon is a liquid drop spreading across a surface when the liquid drop is placed on it, and wetting has attracted particular attention in artificial compound eyes,[19] microlenses,[20] and digital microfluidic devices.[21] At present, there are a lot of research on the macroscopic scale wetting behavior of ILs,[22−28] but the relevant study on the nanowetting behavior of ILs is still relatively scarce. In 2008, Wu and co-workers[29] investigated the microscopic structures of the imidazolium-based IL 1-butyl-3-methylimidazolium hexfluorophosphate ([Bmim][PF_6]) bulk with the size of 55 × 55 × 55 Å on a hydrophobic graphite surface by MD simulation and showed that both the mass and electron densities of the surface-adsorbed ILs are oscillatory. Yan et al.[30] confirmed the analogous density oscillation at the interfacial region between

Received: July 28, 2017
Revised: September 14, 2017
Published: September 27, 2017

DOI: 10.1021/acs.jpcc.7b07474
J. Phys. Chem. C 2017, 121, 23716−23726

imidazolium-based IL [Bmim][PF_6] bulk with dimensions of 63.96 × 63.90 × 86.79 Å and graphite and also demonstrated that the polar groups tend to aggregate, forming a polar network through MD simulation. Madden et al.[31] observed the imidazolium-based IL [Bmim][PF_6] bulk with a size of 32.23 × 34.4 × 109.62 Å confined between graphite walls using a coarse-grained model and found that the high-density peaks occur near the planar graphite surface while the density far away from the graphite surface is similar to the bulk. Laaksonen et al.[32,33] employed a MD simulation to study the microscopic heterogeneous structure of imidazolium-based IL [Bmim][PF_6] with dimensions of 64.96 × 64.96 × 34.37 Å on a hydrophobic graphene surface, and the results indicated that confined ionic groups in interfacial regions are highly heterogeneous and that the imidazolium ring of $Bmim^+$ cations lies preferentially flat on the graphene surface, while its methyl and butyl side chains are elongated along the graphene surface.

There have been few explicit experimental and theoretical reports of the dynamical nanowetting behavior of ILs on the solid surface. In 2013, Heim and Bonaccurso[34] used atomic force microscopy to measure the contact angles of IL droplets with radii between some tens and some hundreds of nanometers on an ideally flat silicon wafer and found that the contact angles decrease with decreasing droplet size (smaller droplets showed stronger wetting), but the dependence of the contact angle on the droplet radius cannot be described with the modified Young−Lippman equation. Rane and Errington[35] employed the Monte Carlo (MC) simulation to probe the role that dispersion and electrostatic interactions played in the wetting behavior of imidazolium-based ILs on nonionic solid substrates, and they showed that the qualitative nature of the wetting behavior is significantly influenced by the competition between dispersion and electrostatic interactions and that the contact angle is nearly independent of temperature over a relatively narrow range of substrate−fluid interaction strengths. Castejón et al.[36] investigated the wetting property of IL droplets with a radius of 25 Å on silanol and silane surfaces and found that the contact angles are much lower than 90° but that the contact angles on the silanol surface are generally slightly lower than those on the silane surface, which is caused by the hydrophilicity difference of these two surfaces. Aparicio and co-workers[37] argued that for 1-ethyl-3-methylimidazolium glycine ([Emim][Gly]) IL nanodroplets on both pure graphene sheets and silica coated with graphene the contact angles are lower than 90° but increase remarkably (from 37° to 81°) when the number of ions pairs varies from 100 to 500. Birkett and co-workers[38] reported the wetting behavior of 1-ethyl-3-methyl-imidazolium tetrafluoroborate ([Emim][BF_4]) IL droplets on graphene sheets and calculated the contact angles via polynomial fitting of two-dimensional atomic density contours, and the results showed that there is no difference in contact angle for drops of different sizes from 100 to 500 IL pairs on a low-potential graphene surface.

However, due to the anisotropic properties of imidazolium-based ILs caused by the asymmetrical distribution of complex cations and anions, the surface of the droplets is no longer a regular spherical surface on the nanoscale. Under such circumstances, the dynamical wetting behavior of droplets needs to be observed in three-dimensional space. In this paper, we take the anisotropic properties of imidazolium-based ILs into consideration and get a complete picture of the nanowetting behavior in three-dimensional space. First, the initial structure of the ensemble is built through placing droplets of three kinds of ILs {1-ethyl-3-methylimidazolium chloride ([Emim][Cl]), 1-ethyl-3-methylimidazolium hexfluorophosphate ([Emim][PF_6]), and [Emim][BF_4]} on the silicon substrate surface. The nanowetting behavior of ILs is probed by observing the spontaneous morphological transition of IL droplets on the silicon surface through simulating the interaction of IL droplets with silicon substrate. Second, using the well-established convex hull algorithm, we give a smoother fit of the drop's surface according to the outermost atomic coordinates in three-dimensional space and find that the fitting surface depends on the type of cation and anion, as different cation and anion can present a different fitting surface. According to the fitting surface, we determine the three-phase contact line (TPCL) along the perimeter of the liquid−solid area and measure the contact angle in different directions. The measured results show that the contact angles present an interesting and significant anisotropy in different directions of the droplets spreading on the solid silicon surface, such as x and y directions. Subsequently, the impact of droplet size, intrinsic viscosity, and temperature of ILs on the nanowetting behavior of an IL nanodroplet on the solid surface is also discussed.

MOLECULAR MODELS AND SIMULATION METHODS

Model. In this study, three kinds of imidazolium-based ILs, [Emim][Cl], [Emim][BF_4] and [Emim][PF_6], are employed to probe the wetting behavior on the nanoscale using MD simulation; the molecular structures of the cation and anions used are shown in Figure 1. The nanowetting behavior is

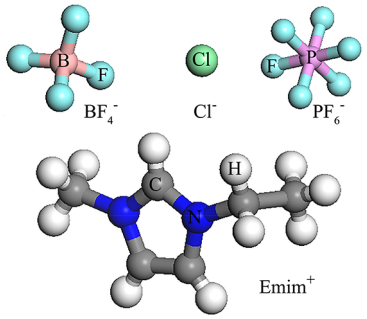

Figure 1. Molecular structures of 1-ethyl-3-methylimidazolium ($Emim^+$), chloride (Cl^-), tetrafluoroborate (BF_4^-), and hexafluorophosphate (PF_6^-).

examined by simulating the interaction of an IL droplet with a solid silicon surface and observing its spontaneous morphological transition into a quasi-hemispherical liquid droplet on the silicon surface. The IL droplet is comprised of some ion pairs initially stacked in a simple spherical structure making use of the PACKMOL software,[39] while the initial structure of the single IL pair is derived from the Cambridge Crystallographic Data Centre (CCDC). For all MD simulations presented in this paper, the radius of IL droplets varies from 10 to 30 Å, such as 10, 15, 20, 25, and 30 Å. The solid silicon substrate with dimensions of 76.8 × 153.6 × 5.76 Å consists of 3200 silicon atoms arranged in a diamond cubic lattice with a lattice constant of 5.46 Å. The solid silicon substrate is frozen during all simulations to enhance computational efficiency. Figure 2 shows the ensemble structure with the initial spherical droplet including 253 [Emim][BF_4] ion pairs obtained from a separate MD simulation, and the radius of the spherical droplet is 25 Å.

DOI: 10.1021/acs.jpcc.7b07474
J. Phys. Chem. C 2017, 121, 23716−23726

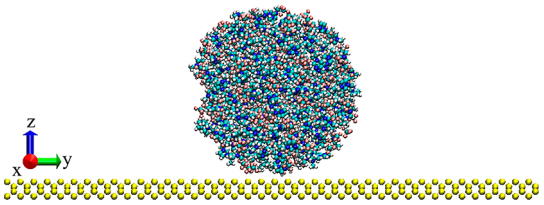

Figure 2. Initial structure of the ensemble.

The size of the simulation box is set as 80 × 160 × 130 Å to avoid interactions with neighbor cells. The bottom surface of the box is fixed to the solid silicon surface, and orthorhombic periodic boundary conditions (PBC) are applied to all three directions of the simulated box during the whole simulation.

Method. All MD simulations are carried out using the general purpose parallel MD simulation open-source package DL_POLY 4.08.[40] Intra- and intermolecular interactions are represented using an all-atom force field developed by Wang and co-workers.[41] The van der Waals (VDW) interaction parameters between different atoms are obtained from the Lorentz−Berthelot combining rules.[42] For a solid silicon substrate, the 12−6 LJ potential parameters are ε = 1.6827 kJ/mol and σ = 3.826 Å.[43]

Unlike other researchers, who started with a cubic structure for ILs and evolved the structure to an equilibrium droplet shape,[36−38] we start directly with a perfectly spherical droplet, which is obtained through a separate MD simulation with gravity neglected. MD simulations are performed under the *NVT* ensemble and a Nosé−Hoover thermostat[44,45] with a relaxation time constant of 1.0 ps applied to the system to maintain the desired constant temperature. The initial velocities are assigned to the atoms randomly according to the system's temperature. The cutoff of the Lennard-Jones and electrostatic interactions is taken as 15 Å. Long-range Coulombic interactions are treated using the smooth particle mesh Ewald (PME) method.[46] The Newton's equation of motion is integrated using a velocity verlet algorithm with an integration time of 2.0 fs. The thermostat is set to the temperature corresponding to the melting point of liquid in the respective system, and the simulation temperature ranges from 300 to 500 K for the studied ILs.

In the results presented below, all final equilibrium states are realized by first equilibrating the IL droplets and the silicon substrate separately. The initial ensemble configurations are equilibrated at the appropriate temperature until the experimental value of the liquid density is achieved; meanwhile, the total energy of the system converges to a constant. The initial configuration of the ensemble consisting of an [Emim][BF_4] droplet and the solid silicon substrate is first equilibrated at T = 300 K for 10 ns. Then the obtained equilibrated configuration at T = 300 K is allowed to run for another 10 ns to ensure a better equilibrium state. Finally, a sample is taken every 1000 time steps to obtain the statistically equilibrated average values in the next 10 ns. Similar simulation procedures are performed with regard to the melting point above 300 K. To ensure that the ILs are in the liquid phase, the equilibrated temperature is T = 350 and 375 K for [Emim][PF_6] and [Emim][Cl], respectively. After the simulation, the physical properties are characterized using the DL_POLY analysis tools, and the structures are visualized with molecular graphics software named Visual Molecular Dynamics (VMD).[47]

RESULTS AND DISCUSSION

Method of Calculating Contact Angles. On the nanoscale, the liquid droplet is no longer an ideal spherical shape and the TPCL is also not a regular circumference. Especially for imidazolium-based ILs, due to the anisotropic properties caused by the asymmetrical distribution of complex cations and anions, the surface of the droplet is rugged (Figure

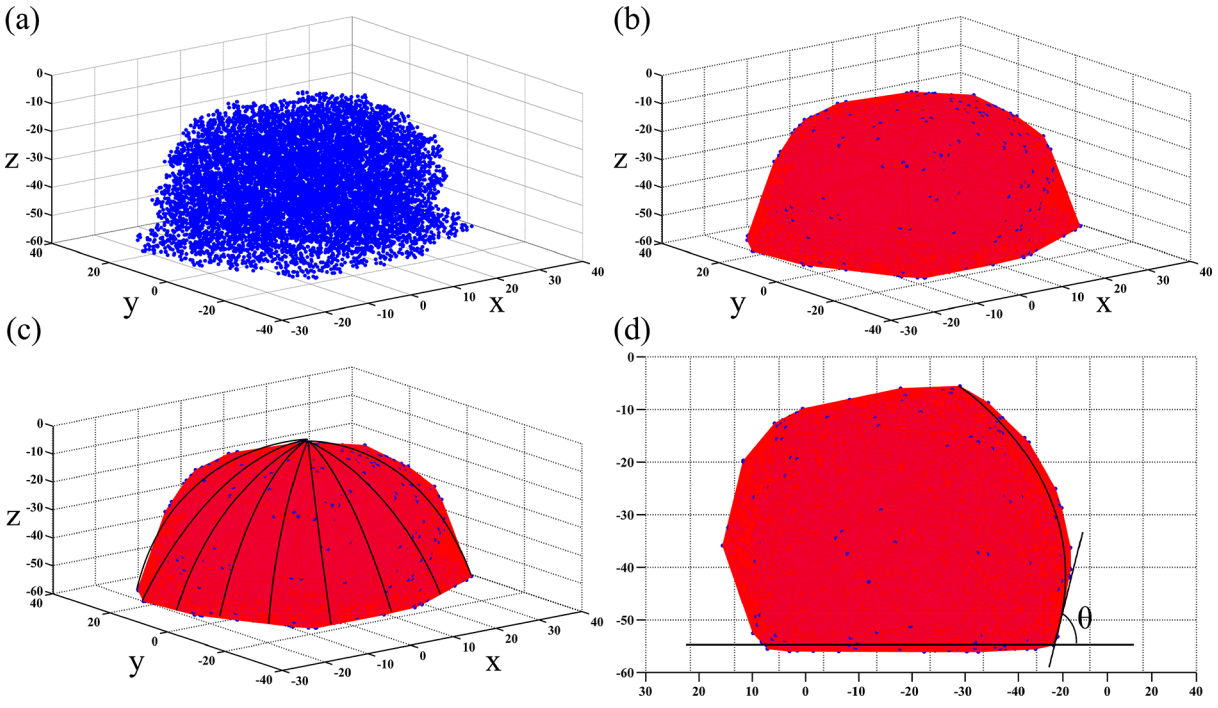

Figure 3. Different steps to calculate the contact angles: (a) the three-dimensional scatter plot of raw data, (b) the three-dimensional surface after fitting raw data, (c) the contact circular arc trajectory in different directions, and (d) measuring the contact angles.

DOI: 10.1021/acs.jpcc.7b07474
J. Phys. Chem. C 2017, 121, 23716−23726

3a). Under such circumstances, it is impossible for the simple two-dimension method to accurately calculate the contact angle and analyze the dynamical nanowetting process. In this section, we use a three-dimensional calculated method to assess the contact angles. As illustrated in Figure 3, first, we draw three-dimensional scatter plot graphs according to atomic coordinates, which are average values obtained from the entire trajectory after the system equilibrates (Figure 3a). To ensure the rationality of the measured contact angles, we do not process the statistical average values. Second, we take advantage of the convex hull algorithm[48] to fit the surface of the droplet and determine the TPCL along the perimeter of the liquid–solid area (Figure 3b). Finally, we measure the contact angle in different directions (Figure 3c,d), and the ultimate value of contact angle is assessed by taking the arithmetic mean of all these measured values.

Droplet Size. On the nanoscale, the droplet size has a profound effect on the wetting behavior of liquids, and the contact angle θ is remarkably size-dependent, as the literature shows.[34,37,38,49] The MD simulations performed with [Emim][BF_4] droplets of different radii of 10, 15, 20, 25, and 30 Å would allow for interference of the effect of nanosizing on the contact angle θ values, and the equilibrated temperature is T = 300 K (the melting point of [Emim][BF_4] is T_{mp} = 286.15 K).[50] The initial liquid configurations reach an equilibrium at the appropriate temperature until the experimental value of the liquid density is obtained; meanwhile, the total energy of the system converges on a constant value and then stays the same [Figure S1, Supporting Information (SI)]. A sample of the final equilibrium state is presented in Figure 4. In the system

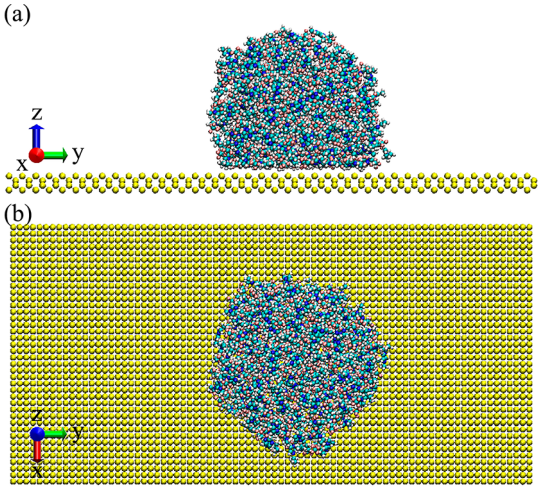

Figure 4. Equilibrium shape of an [Emim][BF_4] droplet with a radius of 25 Å on a silicon surface: (a) side view and (b) top view.

equilibration process, only a few IL ions drift away from the droplet on the silicon substrate, and substantial evaporation is not observed. When all simulation systems attain an equilibrium state, the droplet shape transforms into a quasi-hemisphere.

Figure 5 depicts the contact angle as a function of the radius of the IL droplet at the equilibrium state. Obviously, the contact angle has a significant growth rate as the radius of IL droplets ranged from 10 to 20 Å, and the trend shows agreement with the experimental data.[34] Interestingly and particularly, when the radius is larger than 20 Å, the contact angle increases much more slowly than that of the smaller

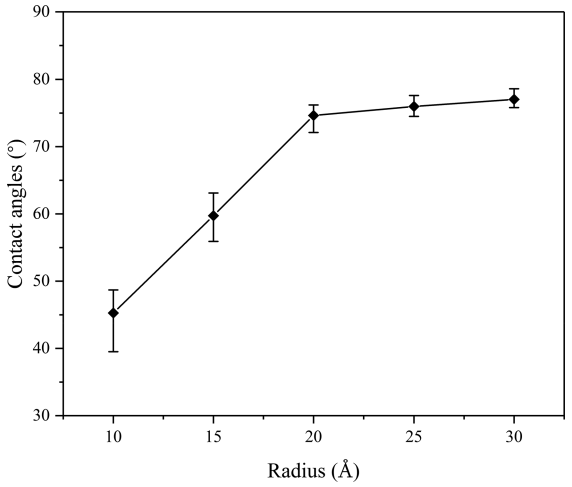

Figure 5. Contact angles of [Emim][BF_4] droplet with different radii on the silicon surface at the equilibrium state. The line is drawn only for guiding purposes.

radius and then tends to be saturated; this is different from the results achieved by the previous works in which the contact angle increases an almost linear manner with the increasing size of the IL droplet.[37] This phenomenon could be due to the strongly adsorbed layer (Figure 6a) forming on the solid surface when the IL droplets are placed on the silicon substrate.[33,37,51] The strongly adsorbed interaction vigorously urges the IL droplet to spread along the solid surface, and it shows good wetting in the presence of remarkable ions–silicon affinity. As shown in Figure 7, for a smaller-radius droplet, the

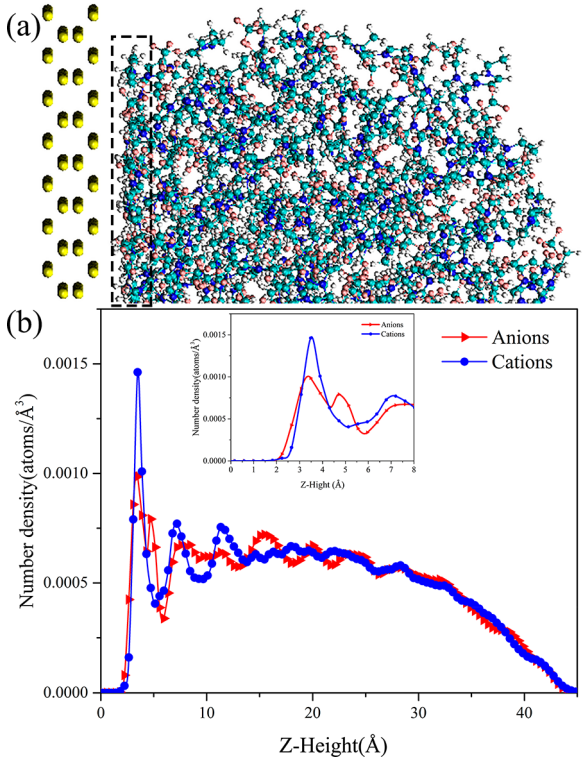

Figure 6. (a) Representative snapshot of the [Emim][BF_4] IL on a solid silicon surface. (b) The number density profiles of cations and anions along the normal direction to the solid silicon surface, where the inset shows the local number density close to the surface.

DOI: 10.1021/acs.jpcc.7b07474
J. Phys. Chem. C 2017, 121, 23716–23726

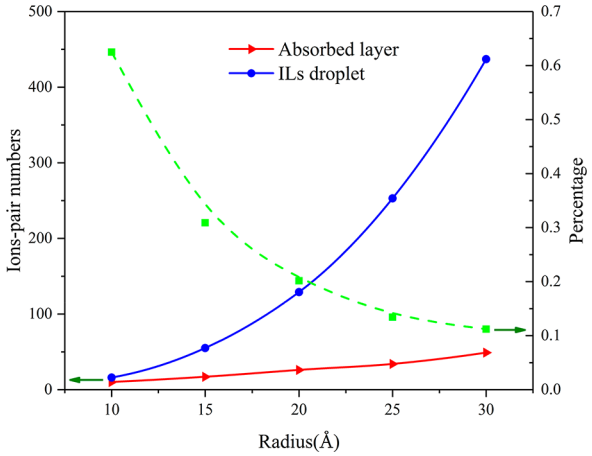

Figure 7. Numbers of ion pairs composing the adsorbed layer with different radii on the silicon surface at the equilibrium state (solid lines) and the proportion of the adsorbed layer ion pairs accounting for the total ion pairs in the droplet (dashed line). The lines are drawn only for guiding purposes.

number of ion pairs that compose the adsorbed layer gradually increases with the increasing IL droplet size, and the strength of the ions−silicon interactions becomes more and more powerful. This is quantified from the MD simulation results using the average ions−silicon intermolecular energies, as showed in Figure 8a, and the stronger ions−silicon interactions result in the greater wetting of the IL droplet and smaller contact angles for a smaller-radius droplet. Nevertheless, when the radius of an IL droplet is beyond 20 Å, additional ion pairs do not tend to be adsorbed on the silicon substrate and the number of ion pairs for the adsorbed layer will not increase rapidly and tend to be saturated; this is confirmed by the results plotted in Figure 7. At this point, the percentage of ion-pair numbers in the adsorbed layer has fallen to 11.2%, and most ions are placed on top of the adsorbed layer on the silicon substrate to increase the interactions of anions−cations through mainly Coulombic forces, as demonstrated by Figure 8b. Therefore, once the number of ion pairs adsorbed on the silicon substrate reaches a critical value, the adsorbed layer is not reinforced by additional ions, because these charged moieties tend to be placed further from the silicon substrate due to the large Coulombic interaction among them, which leads to a saturation of the contact angle. This is confirmed by the calculated contact angles plotted in Figure 5 as a function of the radius of the IL droplet, which increases in an almost linear manner and then tends to be saturated. Moreover, from Figure 8 we can know that the VDW interaction of ions and silicon substrate varies from −56.5 to −53.5 kJ/mol per ion pair and silicon, and the Coulombic interaction of cations and anions varies from −265.3 to −282.0 kJ/mol per ion pair as the droplet radius of ILs ranged from 10 to 30 Å. These differences may be due to the imidazolium ring of cations in the adsorbed layer in the vicinity of the silicon surface being more nearly parallel to the silicon substrate upon increasing the droplet radius, and this allows a very effective interaction with the silicon substrate. The slight changes in structure of the adsorbed layer are showed in Figure S3 (SI).

To further understand the characteristics of the strongly adsorbed layer, analyzing the density distributions along the coordinate perpendicular to the silicon substrate (z direction) is indispensable. Figure 6b presents the density profiles of cations

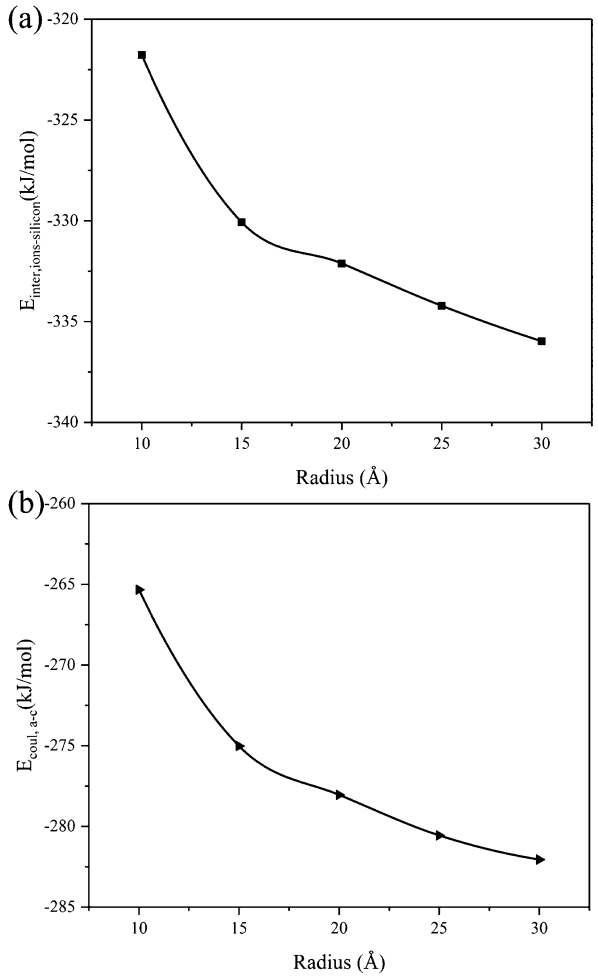

Figure 8. (a) $Emim^+$ and BF_4^- intermolecular interaction energy per ion pair on the solid silicon substrate, $E_{inter,ions-silicon}$. Intermolecular interaction energies are the sum of Lennard-Jones and Coulombic contributions. (b) $Emim^+$ and BF_4^- electrostatic interaction energy per ion pair on the solid silicon substrate, $E_{coul,a-c}$. The lines are drawn only for guiding purposes.

and anions, and the solid surface is placed at $z = 0$. In the case of cations, the number density is obtained from the position of its center of mass (COM), and in the case of anions, from the position of its center of symmetry (boron atom). On the basis of these density profiles, noticeable oscillations are exhibited near the silicon surface and indicate the strongly adsorbed layer forming at the surface. This is apparently attributed to the VDW interactions between ions and silicon that draw IL ions close to the silicon surface, where $Emim^+$ and BF_4^- are packed together to maximize the ions−silicon VDW interactions. However, because the profile of the anions number density at the silicon interface has two separated peaks (Figure 6b, inset) and is much broader compared to that of the cations, $Emim^+$ and BF_4^- are maintained at basically the same number density in the first layer to satisfy the condition of charge neutrality. As illustrated in Figure 6b, the first layer for $Emim^+$ starts around 3.47 Å and has a peak value of 1.46×10^{-3} atoms/Å^3, whereas that for BF_4^- appears around 3.54 Å and has a peak value of 9.86×10^{-4} atoms/Å^3; these values show the larger mass density (~2.42 g/cm^3)[29] in the adsorbed layer, which is nearly doubled compared with the bulk mass density of 1.27 g/cm^3.[52] Hence, in the first layer, there is a rather rigid, or solidlike,

DOI: 10.1021/acs.jpcc.7b07474
J. Phys. Chem. C 2017, 121, 23716−23726

structure formation on the surface due to suppression of their thermal fluctuations. In comparison, at the IL−vacuum interface, although rearrangement of ions reduces the surface energy, which leads to a surface effect, and the number density has a small fluctuation, distinct layering is not observed.[53,54] On the other hand, we also find that the bottom layer structure of the cations is more flat than that of the anions, since the adsorption force of the silicon can induce the alkyl chains and the imidazolium ring of the cations to lie horizontally on the surface. This is quantified through the second-order Legendre polynomials

$$P_2\langle\cos(\theta)\rangle = \frac{1}{2}\langle 3\cos^2(\theta) - 1\rangle \quad (1)$$

where θ is the calculated angle between the vector perpendicular to the silicon substrate (z axis) and selected vectors in both ions. The calculated results are plotted in Figure 9.

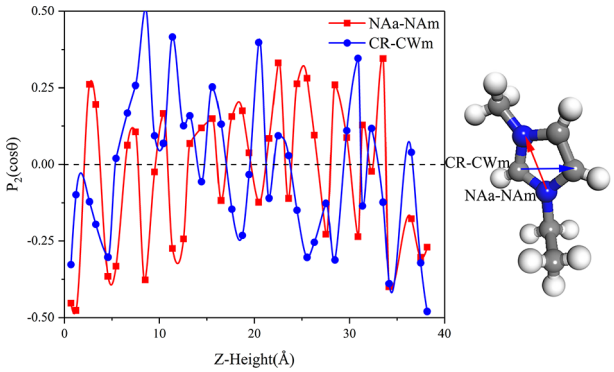

Figure 9. Average $P_2(\cos\theta)$ for the angles between the selected vectors and the silicon substrate normal (z axis) in an [Emim][BF_4] nanodroplet with 25 Å radius.

Furthermore, we find that the values of the contact angle are anisotropic, that is to say, the contact angles are different in each direction of the droplets spreading on the solid silicon surface. The anisotropy of the contact angles could be caused by the inhomogeneous distribution of complex cations and anions, and the increasing radius of the droplets can weaken the anisotropy of the contact angle. For a smaller droplet, the stronger VDW interactions between ions and silicon more easily drag the ions, spreading them on the silicon substrate surface, and the contact angles show strong anisotropy. In contrast, for a larger droplet, the stronger Coulombic interactions between cations and anions make it more difficult to pull ions on the silicon substrate surface, and this weakens the anisotropy of the contact angles. Figure 10 shows the contact angles of an [Emim][BF_4] droplet with different radii on the silicon surface in the x and y directions at the equilibrium state. From Figure 10 we can obviously observe that the contact angle is different in the x and y directions, and the difference value decreases with increasing the droplet radius; that is, the anisotropy of the contact angles becomes weakened as the radius of the IL droplet increased.

Intrinsic Viscosity. The knowledge of the viscosity of ILs is of prime importance for both industrial applications and scientific research. Nevertheless, the viscosity of ILs is much less investigated than other physical quantities such as the density in the nanowetting behavior study, and only limited data are available in the literature. ILs are generally viscous

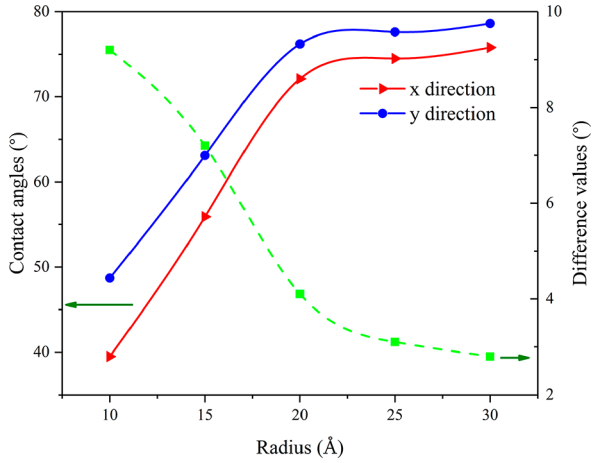

Figure 10. Contact angles of an [Emim][BF_4] droplet with different radii on the silicon surface in the x and y directions at the equilibrium state and the difference between the values of the contact angles in the x and y directions. The lines are drawn only for guiding purposes.

liquids[55,56] with viscosities typically ranging from 10 to 1000 mPa·s at ambient temperature. This is comparable with the values obtained for oils, that is, 2 or 3 orders of magnitude higher than viscosities of traditional molecular organic solvents. This is obviously a real disadvantage for their industrial application and it explains the quest for new ILs exhibiting lower viscosity. Hence, probing the influence of viscosity on nanowetting behavior is required both for industry and academia. In this work, we employ a variety of ILs with different viscosities to anatomize the influence of viscosity on the nanowetting behavior using MD simulation. In order to ensure the rationality of the simulation results, the same equilibrium temperature (T = 400 K) is used for all ILs. Through comparing the simulation results, we find that the IL nanodroplets show a weaker wetting with a higher viscosity; the details are visually presented in Figure 11.

Figure 11 intuitively illustrates that the wetting behavior of different IL nanodroplets exhibits a clear distinction at T = 400 K; it is obvious that the contact angles follow [Emim][Cl] > [Emim][PF_6] > [Emim][BF_4] at T = 400 K, which means that the wetting of ILs is in the sequence of [Emim][Cl] < [Emim][PF_6] < [Emim][BF_4]. At the equilibrium temperature of T = 400 K, the viscosity of ILs containing $Emim^+$ decreases with the following anions: Cl^- > PF_6^- > BF_4^-.[52,57] The results shown in Figure 11 support that the lower viscosity makes IL nanodroplets more wettable and more easily spread on the solid surface because of good fluidity and mobility. Meanwhile, the cations and anions in lower-viscosity ILs can readily come out of initial positions to move toward the solid surface, which leads to greater wetting and smaller contact angles, as demonstrated by Figure 12. Furthermore, for the lower viscosity ILs, the ions−silicon VDW interactions can easily drag the ions out of the nanodroplet and make them adsorb on the solid surface because of the relatively weaker electrostatic interactions between cations and anions. This is quantified from the MD simulation results using the average ions−silicon short-range potential energies through mainly VDW forces and the electrostatic interactions through mainly Coulombic forces plotted in Figure 13. Figures 11 and 12 also illustrate that even for the same IL the contact angle of the droplet will vary with the change in temperature. For Figure 11a,b, the contact angle changes only 2°, which is far lower than the 50° seen in Figure

DOI: 10.1021/acs.jpcc.7b07474
J. Phys. Chem. C 2017, 121, 23716−23726

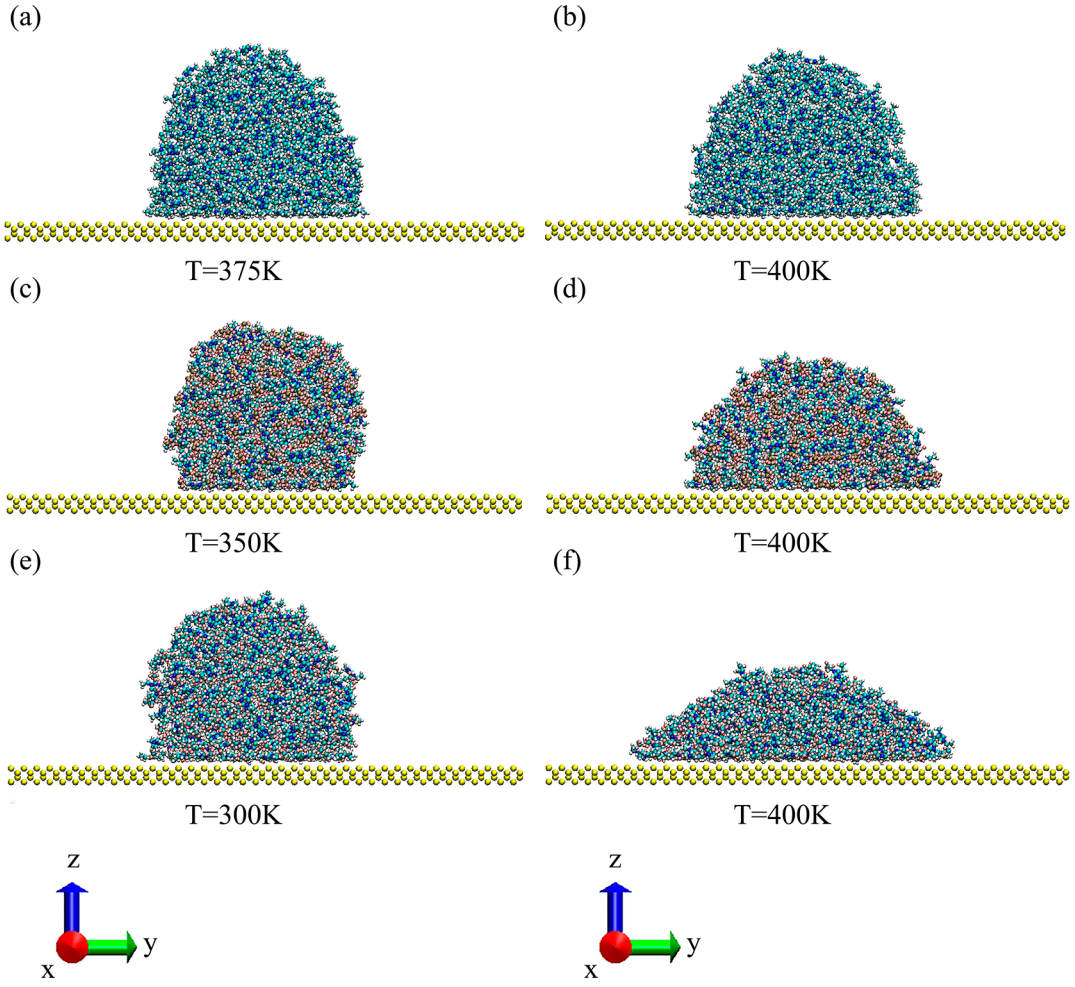

Figure 11. Equilibrium shape of three kinds of IL droplets with a radius of 30 Å on a silicon surface at different temperatures: (a, b) snapshots of [Emim][Cl], (c, d) snapshots of [Emim][PF_6], and (e, f) snapshots of [Emim][BF_4].

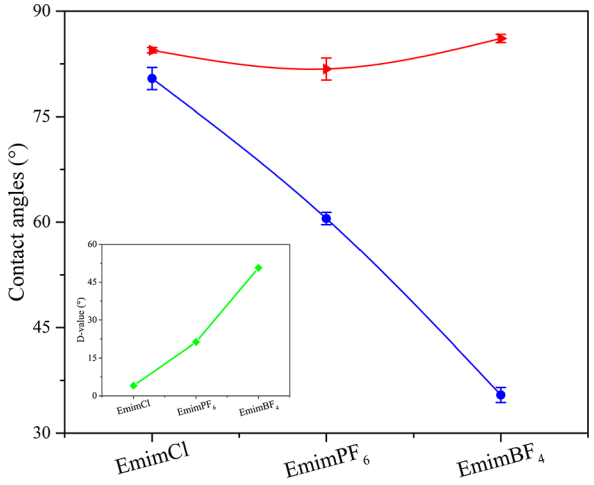

Figure 12. Contact angles for three kinds of IL droplets with a radius of 30 Å on a silicon surface: the triangles represent different temperatures (T = 300, 350, and 375 K for [Emim][BF_4], [Emim][PF_6], [Emim][Cl]), and the circles represent the same temperature (T = 400 K), where the inset shows the D-value of the contact angle at different temperatures. The lines are drawn only for guiding purposes.

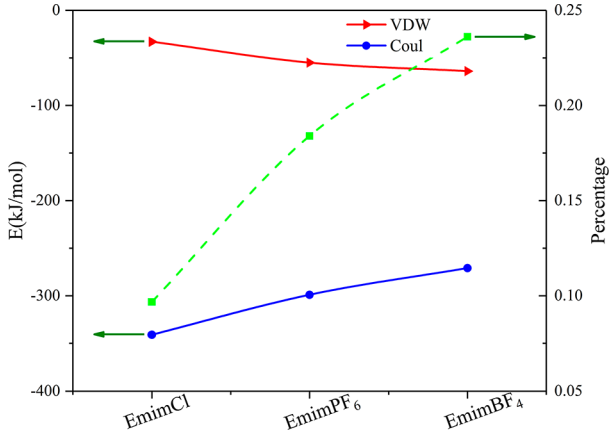

Figure 13. $Emim^+$ and BF_4^- average ions−silicon short-range potential energies ($E_{VDW,a\text{-}c}$) and electrostatic interactions ($E_{coul,a\text{-}c}$) per ion pair on solid silicon substrate (solid lines) and the ratio of $E_{VDW,a\text{-}c}$ to $E_{coul,a\text{-}c}$ (dashed line). Lines are drawn only for guiding purposes.

11e,f, for which the change of temperature is 100 vs 25 K. This behavior can be attributed to the change of the viscosity caused by the different equilibrium temperatures. The scale of the temperature variation determines the range of the change in contact angles.

The mobility of ILs can be seen from the mean square displacements (MSDs)[42] derived from the MD simulation runs. From the molecular point of view, MSDs of molecules give a

DOI: 10.1021/acs.jpcc.7b07474
J. Phys. Chem. C 2017, 121, 23716−23726

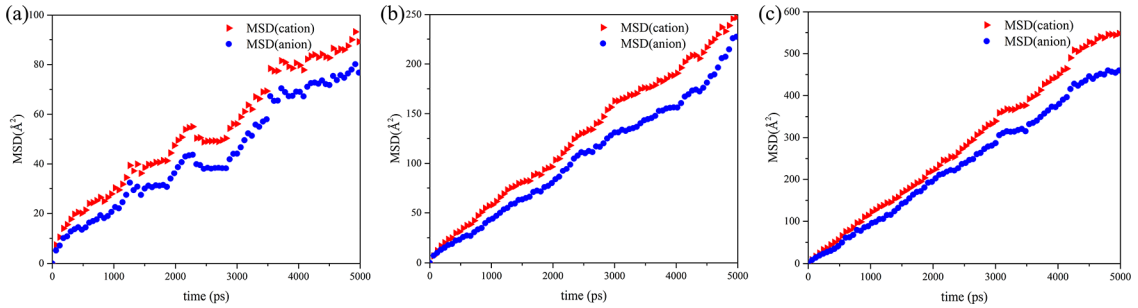

Figure 14. MSDs of imidazolium cations and anions for three ILs at T = 400 K: (a) [Emim][Cl], (b) [Emim][PF_6], and (c) [Emim][BF_4]. The radius for all IL droplets is 30 Å.

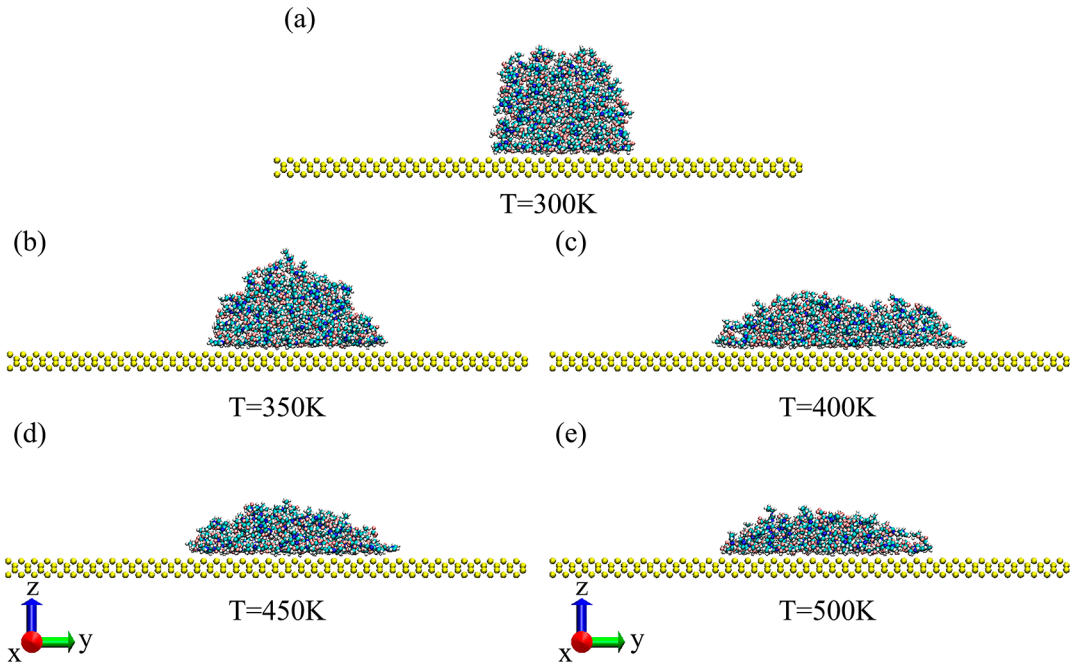

Figure 15. Equilibrium shapes of [Emim][BF_4] IL droplet with a radius of 20 Å on a silicon surface at different temperatures.

detailed microscopic description of single-particle motion. On the nanoscale, the properties of ILs may be different from the bulk system, and the new phenomenon may occur. To study the mobility of IL droplets on the nanoscale, herein, we calculate the corresponding MSDs of different IL droplets, which is defined as

$$\mathrm{MSD} = \frac{1}{N}\langle |r_i^c(t) - r_i^c(0)|^2 \rangle \quad (2)$$

where $r_i^c(t)$ is the COM coordinate of the ith molecule at time t and $r_i^c(0)$ is the initial COM coordinate of the ith molecule at time t = 0. The MSDs of cations and anions for three IL nanodroplets are calculated from trajectories with a time interval 2 ps in the present MD simulations. For the IL nanodroplets consisting of some ion pairs with the same radius at T = 400 K, the calculated MSDs of cations and anions are presented in Figure 14. For different IL nanodroplets, the MSDs of cations and anions are in the order Cl^- < PF_6^- < BF_4^-, which is completely consistent with the change of the contact angle at T = 400 K (Figure 12).

Simulated Temperature. Temperature plays a vital role in the physicochemical properties of ILs and affects the application of ILs in all aspects.[52,58] Understanding the relationship between the wetting behavior of ILs and the temperature is desired to more rationally design and synthesize ILs with an ideal wetting property for the development of industrial processes and daily applications. In this section, an [Emim][BF_4] IL droplet with a radius of 20 Å is employed to explore the influence of temperature on the wetting behavior at different temperatures from 300 to 500 K with intervals of 50 K. All simulation systems are equilibrated after 10 ns from different initial configurations, and the equilibrium shapes are presented in Figure 15.

From Figure 15, we can find that the wetting of ILs is continuously enhanced with the increasing of temperature and eventually reaches a level of saturation. At a lower temperature (Figure 15a), the mobility of IL ions is greatly constrained by the larger viscosity and the cations and anions stay near their original positions. The IL droplet maintains its previous structure very well and presents poor wetting, which gives rise to larger contact angles. Furthermore, the strong electrostatic interactions of cations and anions further intensify the process. It is difficult for ions−silicon VDW interactions to pull the ions to be adsorbed on the solid surface. With the rise of temperature, the viscosity and density of ILs start to decrease[52,59,60] and the wetting of ILs improves obviously. Cations and anions become very active and start to move toward the solid surface under the ions−silicon VDW

DOI: 10.1021/acs.jpcc.7b07474
J. Phys. Chem. C 2017, 121, 23716−23726

interactions with weak constraint coming from the lower viscosity. On the other hand, the decreasing of the density of ILs means the increasing of the volume and results in the lengthening of the distance between cations and anions; thus, the Coulombic force between cations and anions would be weakened so that the ions are more easily dragged toward the solid substrate. More cations and anions are adsorbed on the solid surface, increasing the number of ions existing in the adsorbed layer and maximizing the ions−silicon VDW interactions. Additionally, the liquid surface tension decreases when the temperature increases, while the solid−liquid surface tension relative to the solid surface tension is temperature-independent; it is expected that the contact angle decreases. Under the effect of these key factors, the wetting of IL droplets on the nanoscale will be significantly improved and droplets will present great surface wetting. When the temperature continuously increases to a threshold (∼400 K), the wetting of ILs tends toward saturation. At this time, the quasi-hemispherical IL droplet turns into a liquid film, as illustrated in Figure 15d,e.

CONCLUSION

In summary, here we investigate the dynamical three-dimensional nanowetting behavior of droplets of three kinds of imidazolium-based ILs with different radii ranging from 10 to 30 Å on a solid silicon surface at temperatures varying from 300 to 500 K through a three-dimensional analysis using MD simulation. Using the well-established convex hull algorithm to obtain a smoother fit of the drop's surface according to the outermost atomic coordinates in three-dimensional space, we measure the contact angle in different directions of nanodroplets spreading on the silicon surface and make use of the arithmetic mean of all these measured values as the ultimate value of the contact angle. The measured results indicate that the contact angles change greatly and then tend to be saturated from 45° to 75° as the droplet radius of ILs varied from 10 to 20 Å and further to >20 Å. The values of the contact angle are anisotropic and could be 39.5° and 48.7° in x and y directions of the droplets spreading on the solid silicon surface when the radius of the IL droplet is 10 Å, and increasing the radius of droplets can weaken the anisotropy of the contact angle. Further analysis of the interaction among cations, anions, and silicon suggests that the VDW interaction of ions and silicon substrate varies from −56.5 to −53.5 kJ/mol per ion pair and silicon, and the Coulombic interaction of cations and anions varies from −265.3 to −282.0 kJ/mol per ion pair as the droplet radii of ILs ranged from 10 to 30 Å. These differences may be due to the imidazolium ring of cations in the adsorbed layer in the vicinity of the silicon surface being more nearly parallel to the silicon substrate upon increasing the droplet radius and this allows a very effective interaction with the silicon substrate. For a smaller droplet, the stronger VDW interactions between ions and silicon more easily drag the ions, spreading them on the silicon substrate surface, and the droplet shows greater wetting and strong anisotropy. In contrast, for a larger droplet, the stronger Coulombic interactions of cations and anions make it more difficult to pull ions to the silicon substrate surface, and this weakens the wetting of the IL droplet and the anisotropy of contact angles. Because the total Coulombic interactions of cations and anions and VDW interactions of ions and silicon substrate reach an equilibrium, the contact angles reach a saturation point when the radius of IL droplets is beyond 20 Å. Viscosity plays a critically important role in the nanowetting of IL droplets, and the wetting behavior of IL nanodroplets decreases with the increasing of the viscosity. The nanowetting of IL droplets to a large extent depends on the simulated temperature, and with the increasing of temperature, the nanowetting of IL droplets continuously enhances and eventually reaches a level of saturation when the temperature is T = 400 K, and the quasi-hemispherical IL droplet turns into a liquid film. We hope that the study presented here provides a deeper understanding of the wetting behavior of IL droplets on the nanoscale and can promote the development of nanodevices based on ILs.

ASSOCIATED CONTENT

Supporting Information

The Supporting Information is available free of charge on the ACS Publications website at DOI: 10.1021/acs.jpcc.7b07474.

The variation of the total energy of the simulation system consisting of [Emim][BF_4] and silicon substrate with relaxation time steps, the detailed process to calculate contact angles, the slight changes of the adsorbed layer in the vicinity of the silicon surface, and the contact angles of [Emim][BF_4] droplet with different radii on the silicon surface in the x and y direction at the equilibrium state (PDF)

AUTHOR INFORMATION

Corresponding Authors

*X.Z. e-mail: zxp@lzu.edu.cn.
*Y.D. e-mail: ydeng@licp.cas.cn.

ORCID

Yongji Guan: 0000-0001-9210-3530
Xiaoping Zhang: 0000-0003-0046-211X
Youquan Deng: 0000-0002-7612-0354

Author Contributions

The manuscript was written through contributions of all authors. All authors have given approval to the final version of the manuscript.

Notes

The authors declare no competing financial interest.

ACKNOWLEDGMENTS

The authors acknowledge the financial support of this work from the National Key Research and Development Program of China (2017YFA0403101) and the Fundamental Research Funds for the Central Universities (Nos. lzujbky-2015-306 and Nos. lzujbky-2016-141).

REFERENCES

(1) Wilkes, J. S. A Short History of Ionic Liquids-from Molten Salts to Neoteric Solvents. *Green Chem.* **2002**, *4*, 73−80.

(2) Krossing, I.; Slattery, J. M.; Daguenet, C.; Dyson, P. J.; Oleinikova, A.; Weingärtner, H. Why Are Ionic Liquids Liquid? A Simple Explanation Based on Lattice and Solvation Energies. *J. Am. Chem. Soc.* **2006**, *128*, 13427−13434.

(3) Plechkova, N. V.; Seddon, K. R. Applications of Ionic Liquids in the Chemical Industry. *Chem. Soc. Rev.* **2008**, *37*, 123−150.

(4) Austen Angell, C.; Ansari, Y.; Zhao, Z. Ionic Liquids: Past, Present and Future. *Faraday Discuss.* **2012**, *154*, 9−27.

(5) Anderson, J. L.; Dixon, J. K.; Brennecke, J. F. Solubility of CO_2, CH_4, C_2H_6, C_2H_4, O_2, and N_2 in 1-Hexyl-3-Methylpyridinium Bis(Trifluoromethylsulfonyl)Imide: Comparison to Other Ionic Liquids. *Acc. Chem. Res.* **2007**, *40*, 1208−1216.

DOI: 10.1021/acs.jpcc.7b07474
J. Phys. Chem. C 2017, 121, 23716−23726

(6) Hapiot, P.; Lagrost, C. Electrochemical Reactivity in Room-Temperature Ionic Liquids. *Chem. Rev.* **2008**, *108*, 2238−2264.
(7) Armand, M.; Endres, F.; MacFarlane, D. R.; Ohno, H.; Scrosati, B. Ionic-Liquid Materials for the Electrochemical Challenges of the Future. *Nat. Mater.* **2009**, *8*, 621−629.
(8) Ohno, H. *Electrochemical Aspects of Ionic Liquids*; John Wiley & Sons, 2005.
(9) Hu, X.; Zhang, S.; Qu, C.; Zhang, Q.; Lu, L.; Ma, X.; Zhang, X.; Deng, Y. Ionic Liquid Based Variable Focus Lenses. *Soft Matter* **2011**, *7*, 5941−5943.
(10) Hu, X.; Zhang, S.; Liu, Y.; Qu, C.; Lu, L.; Ma, X.; Zhang, X.; Deng, Y. Electrowetting Based Infrared Lens Using Ionic Liquids. *Appl. Phys. Lett.* **2011**, *99*, 213505.
(11) He, X.; Shao, Q.; Cao, P.; Kong, W.; Sun, J.; Zhang, X.; Deng, Y. Electro-Optical Phenomena Based on Ionic Liquids in an Optofluidic Waveguide. *Lab Chip* **2015**, *15*, 1311−1319.
(12) Kong, W.; Cheng, L.; He, X.; Xu, Z.; Ma, X.; He, Y.; Lu, L.; Zhang, X.; Deng, Y. Electret-Based Microfluidic Power Generator for Harvesting Vibrational Energy by Using Ionic Liquids. *Microfluid. Nanofluid.* **2015**, *18*, 1299−1307.
(13) Shao, Q.; Jia, J.; Guan, Y.; He, X.; Zhang, X. Flow-Induced Voltage Generation by Moving a Nano-Sized Ionic Liquids Droplet over a Graphene Sheet: Molecular Dynamics Simulation. *J. Chem. Phys.* **2016**, *144*, 124703.
(14) Kohagen, M.; Brehm, M.; Lingscheid, Y.; Giernoth, R.; Sangoro, J.; Kremer, F.; Naumov, S.; Iacob, C.; Kärger, J.; Valiullin, R.; et al. How Hydrogen Bonds Influence the Mobility of Imidazolium-Based Ionic Liquids. A Combined Theoretical and Experimental Study of 1-N-Butyl-3-Methylimidazolium Bromide. *J. Phys. Chem. B* **2011**, *115*, 15280−15288.
(15) Migliorati, V.; Serva, A.; Aquilanti, G.; Olivi, L.; Pascarelli, S.; Mathon, O.; D'Angelo, P. Combining Exafs Spectroscopy and Molecular Dynamics Simulations to Understand the Structural and Dynamic Properties of an Imidazolium Iodide Ionic Liquid. *Phys. Chem. Chem. Phys.* **2015**, *17*, 2464−2474.
(16) Migliorati, V.; Serva, A.; Aquilanti, G.; Pascarelli, S.; D'Angelo, P. Local Order and Long Range Correlations in Imidazolium Halide Ionic Liquids: A Combined Molecular Dynamics and Xas Study. *Phys. Chem. Chem. Phys.* **2015**, *17*, 16443−16453.
(17) Červinka, C.; Pádua, A. A. H.; Fulem, M. Thermodynamic Properties of Selected Homologous Series of Ionic Liquids Calculated Using Molecular Dynamics. *J. Phys. Chem. B* **2016**, *120*, 2362−2371.
(18) Zhang, S.; Zhang, J.; Zhang, Y.; Deng, Y. Nanoconfined Ionic Liquids. *Chem. Rev.* **2017**, *117*, 6755−6833.
(19) Ko, D. H.; Tumbleston, J. R.; Henderson, K. J.; Euliss, L. E.; DeSimone, J. M.; Lopez, R.; Samulski, E. T. Biomimetic Microlens Array with Antireflective "Moth-Eye" Surface. *Soft Matter* **2011**, *7*, 6404−6407.
(20) Nagelberg, S.; Zarzar, L. D.; Nicolas, N.; Subramanian, K.; Kalow, J. A.; Sresht, V.; Blankschtein, D.; Barbastathis, G.; Kreysing, M.; Swager, T. M.; et al. Reconfigurable and Responsive Droplet-Based Compound Micro-Lenses. *Nat. Commun.* **2017**, *8*, 14673.
(21) Preston, D. J.; Anders, A.; Barabadi, B.; Tio, E.; Zhu, Y.; Dai, D. A.; Wang, E. N. Electrowetting-on-Dielectric Actuation of a Vertical Translation and Angular Manipulation Stage. *Appl. Phys. Lett.* **2016**, *109*, 244102.
(22) Eberhart, J. The Wetting Behavior of Dialkylimidazolium Chloroaluminate, a Room Temperature Molten Salt. *J. Electrochem. Soc.* **1985**, *132*, 1889.
(23) Millefiorini, S.; Tkaczyk, A. H.; Sedev, R.; Efthimiadis, J.; Ralston, J. Electrowetting of Ionic Liquids. *J. Am. Chem. Soc.* **2006**, *128*, 3098−3101.
(24) Batchelor, T.; Cunder, J.; Fadeev, A. Y. Wetting Study of Imidazolium Ionic Liquids. *J. Colloid Interface Sci.* **2009**, *330*, 415−420.
(25) Restolho, J.; Mata, J. L.; Saramago, B. Electrowetting of Ionic Liquids: Contact Angle Saturation and Irreversibility. *J. Phys. Chem. C* **2009**, *113*, 9321−9327.
(26) Paneru, M.; Priest, C.; Sedev, R.; Ralston, J. Electrowetting of Aqueous Solutions of Ionic Liquid in Solid−Liquid−Liquid Systems. *J. Phys. Chem. C* **2010**, *114*, 8383−8388.
(27) Paneru, M.; Priest, C.; Sedev, R.; Ralston, J. Static and Dynamic Electrowetting of an Ionic Liquid in a Solid/Liquid/Liquid System. *J. Am. Chem. Soc.* **2010**, *132*, 8301−8308.
(28) Sedev, R. Surface Tension, Interfacial Tension and Contact Angles of Ionic Liquids. *Curr. Opin. Colloid Interface Sci.* **2011**, *16*, 310−316.
(29) Maolin, S.; Fuchun, Z.; Guozhong, W.; Haiping, F.; Chunlei, W.; Shimou, C.; Yi, Z.; Jun, H. Ordering Layers of [Bmim][PF_6] Ionic Liquid on Graphite Surfaces: Molecular Dynamics Simulation. *J. Chem. Phys.* **2008**, *128*, 134504.
(30) Wang, S.; Li, S.; Cao, Z.; Yan, T. Molecular Dynamic Simulations of Ionic Liquids at Graphite Surface. *J. Phys. Chem. C* **2010**, *114*, 990−995.
(31) Merlet, C.; Salanne, M.; Rotenberg, B.; Madden, P. A. Imidazolium Ionic Liquid Interfaces with Vapor and Graphite: Interfacial Tension and Capacitance from Coarse-Grained Molecular Simulations. *J. Phys. Chem. C* **2011**, *115*, 16613−16618.
(32) Wang, Y. L.; Laaksonen, A.; Lu, Z. Y. Influence of Ionic Liquid Film Thickness on Ion Pair Distributions and Orientations at Graphene and Vacuum Interfaces. *Phys. Chem. Chem. Phys.* **2013**, *15*, 13559−13569.
(33) Wang, Y. L.; Lu, Z. Y.; Laaksonen, A. Heterogeneous Dynamics of Ionic Liquids in Confined Films with Varied Film Thickness. *Phys. Chem. Chem. Phys.* **2014**, *16*, 20731−20740.
(34) Heim, L. O.; Bonaccurso, E. Measurement of Line Tension on Droplets in the Submicrometer Range. *Langmuir* **2013**, *29*, 14147−14153.
(35) Rane, K. S.; Errington, J. R. Understanding the Influence of Coulomb and Dispersion Interactions on the Wetting Behavior of Ionic Liquids. *J. Chem. Phys.* **2014**, *141*, 174706.
(36) Castejón, H. J.; Wynn, T. J.; Marcin, Z. M. Wetting and Tribological Properties of Ionic Liquids. *J. Phys. Chem. B* **2014**, *118*, 3661−3668.
(37) Herrera, C.; García, G.; Atilhan, M.; Aparicio, S. Nanowetting of Graphene by Ionic Liquid Droplets. *J. Phys. Chem. C* **2015**, *119*, 24529−24537.
(38) Burt, R.; Birkett, G.; Salanne, M.; Zhao, X. S. Molecular Dynamics Simulations of the Influence of Drop Size and Surface Potential on the Contact Angle of Ionic-Liquid Droplets. *J. Phys. Chem. C* **2016**, *120*, 15244−15250.
(39) Martínez, L.; Andrade, R.; Birgin, E. G.; Martínez, J. M. PACKMOL: A Package for Building Initial Configurations for Molecular Dynamics Simulations. *J. Comput. Chem.* **2009**, *30*, 2157−2164.
(40) Todorov, I. T.; Smith, W.; Trachenko, K.; Dove, M. T. DL_POLY_3: New Dimensions in Molecular Dynamics Simulations Via Massive Parallelism. *J. Mater. Chem.* **2006**, *16*, 1911−1918.
(41) Liu, Z.; Huang, S.; Wang, W. A Refined Force Field for Molecular Simulation of Imidazolium-Based Ionic Liquids. *J. Phys. Chem. B* **2004**, *108*, 12978−12989.
(42) Allen, M. P.; Tildesley, D. J. *Computer Simulation of Liquids*; Oxford University Press, 1989.
(43) Yang, Z.; Lu, Z. Atomistic Simulation of the Mechanical Behaviors of Co-Continuous Cu/Sic Nanocomposites. *Composites, Part B* **2013**, *44*, 453−457.
(44) Nosé, S. A Unified Formulation of the Constant Temperature Molecular Dynamics Methods. *J. Chem. Phys.* **1984**, *81*, 511−519.
(45) Hoover, W. G. Canonical Dynamics: Equilibrium Phase-Space Distributions. *Phys. Rev. A: At., Mol., Opt. Phys.* **1985**, *31*, 1695−1697.
(46) Essmann, U.; Perera, L.; Berkowitz, M. L.; Darden, T.; Lee, H.; Pedersen, L. G. A Smooth Particle Mesh Ewald Method. *J. Chem. Phys.* **1995**, *103*, 8577−8593.
(47) Humphrey, W.; Dalke, A.; Schulten, K. Vmd: Visual Molecular Dynamics. *J. Mol. Graphics* **1996**, *14*, 33−38.

DOI: 10.1021/acs.jpcc.7b07474
J. Phys. Chem. C 2017, 121, 23716−23726

(48) Barber, C. B.; Dobkin, D. P.; Huhdanpaa, H. The Quickhull Algorithm for Convex Hulls. *ACM Trans. Math. Softw.* **1996**, *22*, 469−483.
(49) Santiso, E. E.; Herdes, C.; Müller, A. E. On the Calculation of Solid-Fluid Contact Angles from Molecular Dynamics. *Entropy* **2013**, *15*, 3734−3745.
(50) Nishida, T.; Tashiro, Y.; Yamamoto, M. Physical and Electrochemical Properties of 1-Alkyl-3-Methylimidazolium Tetrafluoroborate for Electrolyte. *J. Fluorine Chem.* **2003**, *120*, 135−141.
(51) Kislenko, S. A.; Samoylov, I. S.; Amirov, R. H. Molecular Dynamics Simulation of the Electrochemical Interface between a Graphite Surface and the Ionic Liquid [Bmim][PF_6]. *Phys. Chem. Chem. Phys.* **2009**, *11*, 5584−5590.
(52) Shamsipur, M.; Beigi, A. A. M.; Teymouri, M.; Pourmortazavi, S. M.; Irandoust, M. Physical and Electrochemical Properties of Ionic Liquids 1-Ethyl-3-Methylimidazolium Tetrafluoroborate, 1-Butyl-3-Methylimidazolium Trifluoromethanesulfonate and 1-Butyl-1-Methyl-pyrrolidinium Bis(Trifluoromethylsulfonyl)Imide. *J. Mol. Liq.* **2010**, *157*, 43−50.
(53) Bhargava, B. L.; Balasubramanian, S. Layering at an Ionic Liquid−Vapor Interface: A Molecular Dynamics Simulation Study of [Bmim][PF_6]. *J. Am. Chem. Soc.* **2006**, *128*, 10073−10078.
(54) Lynden-Bell, R. M.; Del Popolo, M. Simulation of the Surface Structure of Butylmethylimidazolium Ionic Liquids. *Phys. Chem. Chem. Phys.* **2006**, *8*, 949−954.
(55) Wilkes, J. S. Properties of Ionic Liquid Solvents for Catalysis. *J. Mol. Catal. A: Chem.* **2004**, *214*, 11−17.
(56) Marsh, K. N.; Boxall, J. A.; Lichtenthaler, R. Room Temperature Ionic Liquids and Their Mixtures—A Review. *Fluid Phase Equilib.* **2004**, *219*, 93−98.
(57) Seddon, K. R.; Stark, A.; Torres, M. J. Viscosity and Density of 1-Alkyl-3-Methylimidazolium Ionic Liquids. In *Clean Solvents*; American Chemical Society, 2002; Vol. *819*, pp 34−49.
(58) Fredlake, C. P.; Crosthwaite, J. M.; Hert, D. G.; Aki, S. N. V. K.; Brennecke, J. F. Thermophysical Properties of Imidazolium-Based Ionic Liquids. *J. Chem. Eng. Data* **2004**, *49*, 954−964.
(59) Ghatee, M. H.; Zare, M.; Zolghadr, A. R.; Moosavi, F. Temperature Dependence of Viscosity and Relation with the Surface Tension of Ionic Liquids. *Fluid Phase Equilib.* **2010**, *291*, 188−194.
(60) Okoturo, O. O.; VanderNoot, T. J. Temperature Dependence of Viscosity for Room Temperature Ionic Liquids. *J. Electroanal. Chem.* **2004**, *568*, 167−181.

DOI: 10.1021/acs.jpcc.7b07474
J. Phys. Chem. C 2017, 121, 23716−23726